

Novel application of [¹⁸F]DPA714 for visualizing the pulmonary inflammation process of SARS-CoV-2-infection in rhesus monkeys (*Macaca mulatta*)

Lisette Meijer^{a,1}, Kinga P. Böszörményi^{a,1}, Jaco Bakker^a, Gerrit Koopman^a, Petra Mooij^a, Dagmar Verel^a, Zahra Fagrouch^a, Babs E. Verstrepen^a, Uta Funke^c, Martien P.J. Mooijer^c, Jan A.M. Langermans^{a,b}, Ernst J. Verschoor^a, Albert D. Windhorst^c, Marieke A. Stammes^{a,*}

^a Biomedical Primate Research Centre (BPRC), Rijswijk, Netherlands

^b Population Health Sciences, Veterinary Faculty, Utrecht University, Utrecht, Netherlands

^c Department of Radiology and Nuclear Medicine, Tracer Center Amsterdam (TCA), Amsterdam UMC, Vrije Universiteit, Amsterdam, Netherlands

ARTICLE INFO

Keywords:

TSPO
Pulmonary inflammation
PET-CT
COVID-19
Nonhuman primates

ABSTRACT

Rationale: The aim of this study was to investigate the application of [¹⁸F]DPA714 to visualize the inflammation process in the lungs of SARS-CoV-2-infected rhesus monkeys, focusing on the presence of pulmonary lesions, activation of mediastinal lymph nodes and surrounded lung tissue.

Methods: Four experimentally SARS-CoV-2 infected rhesus monkeys were followed for seven weeks post infection (pi) with a weekly PET-CT using [¹⁸F]DPA714. Two PET images, 10 min each, of a single field-of-view covering the chest area, were obtained 10 and 30 min after injection. To determine the infection process swabs, blood and bronchoalveolar lavages (BALs) were obtained.

Results: All animals were positive for SARS-CoV-2 in both the swabs and BALs on multiple timepoints pi. The initial development of pulmonary lesions was already detected at the first scan, performed 2-days pi. PET revealed an increased tracer uptake in the pulmonary lesions and mediastinal lymph nodes of all animals from the first scan obtained after infection and onwards. However, also an increased uptake was detected in the lung tissue surrounding the lesions, which persisted until day 30 and then subsided by day 37–44 pi. In parallel, a similar pattern of increased expression of activation markers was observed on dendritic cells in blood.

Principal conclusions: This study illustrates that [¹⁸F]DPA714 is a valuable radiotracer to visualize SARS-CoV-2-associated pulmonary inflammation, which coincided with activation of dendritic cells in blood. [¹⁸F]DPA714 thus has the potential to be of added value as diagnostic tracer for other viral respiratory infections.

1. Introduction

Molecular imaging provides, in a non-invasive manner, three-dimensional data of a region of interest of the entire body. A spatio-temporal visualization of the region of interest can be obtained longitudinally within the same individual [1]. Multiple new radiotracers have been developed, predominantly for oncology and neurology, but also for imaging inflammatory processes. One of the molecular targets for imaging inflammation for which radiotracers are developed is the mitochondrial translocator-protein (TSPO). TSPO is widely distributed over the entire body but is upregulated in activated microglia and systemic

monocytes. Until now its application has been mainly limited to imaging of neuroinflammatory purposes; multiple TSPO tracers have been developed and are successfully used in, for instance, in patients with Multiple Sclerosis or Alzheimer's Disease [2–6]. However, as TSPO is distributed over the entire body, the radiotracer may visualize inflammatory processes in other organs than the brain as well. This makes TSPO a valuable tool to visualize the progress in infectious diseases, and in this regard focused on, respiratory infections [7–10].

One endemic disease for which it is of utmost importance to gain more insights in the disease progress, is coronavirus disease 2019 (COVID-19), caused by severe acute respiratory syndrome coronavirus 2

* Corresponding author at: Lange Kleiweg 161, 2288GJ Rijswijk, Netherlands.

E-mail address: stammes@bprc.nl (M.A. Stammes).

¹ These authors contributed equally.


Day	-5	0	1	2	3	4	5	6	8	10	12	16	23	30	37	44
Infection																
PET-CT																
Swabs																
Blood samples																
BAL																

Fig. 1. Schematic overview of the experimental procedures within the study, related to this manuscript.

(SARS-CoV-2). Syrian hamsters (*Mesocricetus auratus*) and nonhuman primates (NHPs) are used as models for SARS-CoV-2 infection and visualization of the respiratory tract infection [10–12]. Both species are established animal models to study COVID-19 as the distribution of angiotensin converting enzyme 2 (ACE2), the cellular receptor of SARS-CoV-2, in these species is comparable to humans. In addition, it has been shown that both animal models reproduce phenotypic aspects of symptomatic SARS-CoV-2 infection in humans [13,14]. However, due to anatomic uniformness NHPs to humans, NHPs have an advantage over Syrian hamsters in imaging studies.

A hallmark of COVID-19 is lower respiratory tract infection. In humans, pulmonary injury is predominantly evaluated using noninvasive medical imaging procedures, most commonly a chest X-ray (CXR) or chest computed tomography (CT). In NHPs the added benefit of medical imaging to characterize and quantify disease has been demonstrated [12]. However, CXR, CT, and current positron emission tomography (PET) tracers can only visualize pulmonary lesions and activated lymph nodes when they are evident, but visualization of the early and ongoing infection process and its development in time is challenging. Noninvasive visualization of the entire pulmonary tract via molecular imaging with a dedicated PET tracer may shed light on the developmental pattern of the infection process.

Pulmonary lesions are induced by replicating virus in the epithelial cells causing cell death accompanied by the infiltration of immune cells, like macrophages and monocytes, into alveolar septa and lumina [15]. By monitoring immune infiltrates with a radiotracer directed towards TSPO, we might be able to visualize the first stage of pulmonary inflammation, before cell death occurs. This will provide information about the initiation of the local inflammatory process, especially in the lower respiratory tract, after a SARS-CoV-2 infection. In this regard, TSPO can be of relevance, as monitoring of pulmonary immune infiltrates may aid in the early identification of patients developing severe forms of COVID-19 disease and could add to the development of early therapeutic interventions.

In this proof-of-concept study, we applied [¹⁸F]DPA714 as tracer for TSPO to study inflammatory processes in the pulmonary tract of macaques, experimentally infected with SARS-CoV-2.

2. Materials and methods

2.1. Ethics approval

This study was performed at the Biomedical Primate Research Centre (BPRC, Rijswijk, Netherlands) under project license AVD5020020209404 which was issued by the competent national authorities (Central Committee for Animal Experiments). Further approval was obtained after assessment of the study protocol by the institutional animal welfare body. All procedures, husbandry, and housing were performed in accordance with the Dutch laws on animal experimentation and the EU Directive 63/2010. The BPRC is accredited by the

American Association for Accreditation of Laboratory Animal Care (AAALAC) International.

2.2. Animals

Four healthy Indian-origin male rhesus monkeys (*Macaca mulatta*) (age 4–7y, weight 8.2–9.6 kg) were selected from the breeding colony of the Biomedical Primate Research Centre (BPRC, Rijswijk, Netherlands). All animals were classified healthy according to physical examination and the evaluation of complete blood count and serum chemistry before the start of each study. A complete physical, hematological, and biochemical evaluation was performed on the animals before inclusion in the study.

The animals were socially housed, in pairs, during the study. The monkeys were offered a daily diet consisting of commercial monkey pellets (Ssniff, Soest, Germany) supplemented with vegetables and fruit. Homemade or commercially available enrichment products were provided daily. Drinking water was available ad libitum via an automatic watering system. Animal care staff provided daily visual health checks. The animals were monitored for appetite, general behavior, and stool consistency. In addition, any abnormalities related to an airway infection like sneezing, coughing, dyspnea and breathing frequency were noted. All possible precautions were taken to ensure the welfare and to avoid any discomfort to the animals. At the end of the study the animals were euthanized.

2.3. Virus, experimental infection, and post-exposure study follow-up

All experimental interventions (intratracheal and intranasal infection, swab collections, blood samplings, bronchoalveolar lavages (BALs) and PET-CTs) were performed under anesthesia till 44 days post infection (pi) (for details: Fig. 1). The animals were exposed with SARS-CoV-2 strain hCoV-19/Netherlands/NH-RIVM-27142/2021 (Delta variant, lineage B.1.617.2) that was made available through the European Virus Archive-Global (EVAg). The macaques were inoculated with a dose of 1×10^5 TCID₅₀, diluted in 5 ml phosphate-buffered saline (PBS), via a combined intratracheal, just below the vocal cords, (4.5 ml) and intranasal (0.25 ml in each nostril) route [1]. Ethylenediaminetetraacetic acid (EDTA) blood was collected using standard aseptic methods at regular time points pi for fluorescence activated cell sorting (FACS) analysis (Fig. 1), and in parallel, tracheal, and nasal swabs were taken. In addition, at three pre-defined timepoints pi, a BAL of the lower left lung was obtained to determine viral load [16,17]. The determination of the presence of SARS-CoV-2 RNA in the swabs, blood and BAL was performed as described previously [1].

2.4. FACS analysis

Multiparameter FACS analysis was performed using a monoclonal antibody (mAb) panel to measure activation in blood [18]. The

following mAb combinations, relevant for this manuscript, were used: CD45^{BUV496} (Becton & Dickinson, Franklin Lakes, NJ, USA (BD), cat 741185), HLA-DR^{BUV805} (BD, cat 748338), CD20^{V450} (BD, cat 655872), CD16^{BV605} (BD, cat 563916), CD3^{BV650} (BD, 563916), CD40^{BV750} (BD, cat 746948), CD14^{PE-TxRed} (Beckman Coulter, cat B92391), CD123^{PerCP-Cy5.5} (BD cat 558714), CD86^{Alexa647} (Biolegend, San Diego, CA, USA, cat 305416), CD1c^{APC} (Ebioscience cat 17-0015-42). Acquisition was performed on an Aurora flow cytometer (Cytex, Fremont, Ca, USA) and analyzed using FlowJo software. For analysis, the CD45 positive cells with a low side scatter (SSC) profile were first gated and then singlets were selected using a forward scatter (FSC) height versus area plot. Then, HLA-DR positive/CD3, CD20 and CD14 negative cells were selected and CD123 was plotted against CD1c to identify the plasmacytoid DC (pDC)(CD123 positive/CD1c negative) and classical DC2 (cDC2)(CD123 negative/CD1c positive) populations. Expression of CD40 and CD86 was quantified as the mean geometric mean of the fluorescence intensity (MFI).

2.5. Radiosynthesis of [¹⁸F]DPA714

Radiosynthesis of [¹⁸F]DPA714 was performed using procedures described previously [19] using in-house built automatic devices. [¹⁸F]DPA714 was produced with a molar activity of 77.4 GBq/μmol (range 39.8–150.6 GBq/μmol on activity reference time (ART)), a radioactivity concentration of 277.0 ± 172.8 MBq/ml, and a radiochemical purity of at least 98.0%.

2.6. PET-CT acquisition, reconstruction, and analysis

A PET-CT was acquired pre-infection (day –5) to obtain a baseline value. Weekly PET-CTs were obtained (Fig. 1) using a MultiScan Large Field of View Extreme Resolution Research Imager (LFER) 150 PET-CT (Mediso Medical Imaging Systems Ltd., Budapest, Hungary) as described before [20]. Animals were fasted overnight and were sedated with ketamine (10 mg/kg ketamine hydrochloride (Alfasan Nederland BV, Woerden, Netherlands) combined with medetomidine hydrochloride (0.05 mg/kg (Sedastart; AST Farma B.V., Oudewater, Netherlands), both administrated intramuscularly. The animals were positioned head-first supine (HFS) with the arms up. After the scan, upon return to their home cage, atipamezole hydrochloride (Sedastop, ASTFarma B.V., Oudewater, Netherlands, 5 mg/ml, 0.25 mg/kg) was administrated intramuscular to antagonize medetomidine.

Following a scout-view, an intravenous bolus (1–2 ml) of approximately 180 MBq [¹⁸F]DPA714 was administered. Two PET images, 10 min each, of a single field-of-view covering the chest area, were obtained 10 and 30 min after injection. Afterwards a CT was obtained to use for both diagnostic evaluation of the pulmonary tract and attenuation correction. The system utilizes cone-beam CT technology which covers a volume of 150 × 200 × 200 mm³ in a single rotation of 32.4 s. For each scan 3 rotations of 480 projections each were captured. The main scan parameters applied for scans used in this manuscript were 80 kV, 720 μA and an exposure time of 0.09 s. The CT was retrospectively gated in the expiration phase and afterwards reconstructed following a filtered back projection (FBP) protocol with a RamLak filter and an isotropic voxel size of 321 μm. The CT was captured both for diagnostic evaluation and fusion with the PET as described previously [21]. The emission data were iteratively reconstructed (OSEM3D, 8 iterations and 9 subsets with an isotropic voxel size of 0.8 mm) into a single frame PET image normalized and corrected for attenuation, scatter, and random coincidences using the free-breathing CT, and corrected for radioactive decay. The analysis was performed with VivoQuant 4.5 (Invivo, Boston, USA). The uptake in the pulmonary lesions and lymph nodes was quantified using a lower threshold standard uptake value (SUV) of 3.0 to discriminate from the surrounding tissue. No differentiation by CT density was applied for discriminating the lesions in the lungs as the difference in density of the pulmonary lesions compared to the

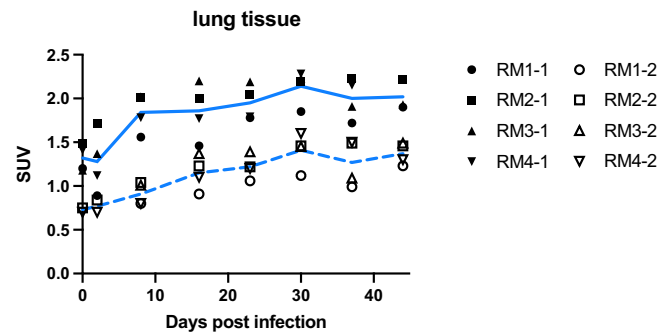


Fig. 2. Development of the SUVmean in the anatomically unaffected lung tissue over time. The dots represent the separate animals (filled symbols = scan 1 obtained 10 min post injection, open symbols = scan 2 obtained 30 min post injection). The continuous line indicates the average of scan 1 and the dotted line of scan 2.

surrounding lung tissue is only minimal for ground glass opacities (GGOs). A density range was only applied on the CT for defining the lungs (–1000/–400 Hounsfield units (HU)). To prevent possible spill-over effects of the myocardium and liver an additional boundary around these structures is used to subtract from the region-of-interest.

For statistical analysis, a two-sided paired *t*-test or a Spearman correlation was performed, *p*-values <0.05 were considered significant.

3. Results

3.1. Virus infection

Following the exposure of SARS-CoV-2, viral RNA was detected in all macaques from day 1 pi up to 14 days pi in the tracheal and nasal swab samples. The detection of subgenomic messenger RNA (sgmRNA) in tracheal and nasal swabs from all animals at multiple time points indicated the presence of replicating virus up to 10 days pi. BAL samples collected at days 3 and 6 pi were positive for viral RNA. No sgmRNA was detected in blood samples, denoting the absence of active virus replication in blood. During the entire study, only minor clinical signs putatively related to COVID-19 were noticed in the animals, i.e. an occasional cough.

3.2. Imaging of the pulmonary tract

3.2.1. Lung tissue

Lung tissue was determined as the entire lung volume defined by the density range (–1000 HU/–400HU) minus the lung lesions in this area as demarcated by the SUV threshold. The density and volume of the lungs remained roughly the same over the entire experiment with a strong correlation ($r = -0.824$, $p < 0.0001$). An increase in [¹⁸F]DPA714 PET uptake was detected in the lung tissue surrounding the lung lesions, which is anatomically unaffected, after SARS-CoV-2 infection and this increase continued over the entire observation period and peaked at 30 days pi after which it reached a plateau. At that day an average increase in SUVmean of 0.82 for the scan was obtained at 10-minutes post injection, after which it stabilized. In the second scan, obtained 30 min post injection, a similar pattern was observed with an average increase in SUVmean of 0.68 (Fig. 2). This is an increase of 61.93% and 93.63% respectively for scan 1 and scan 2 compared to baseline values. No correlations were observed for the SUVmean vs density ($r = -0.024$, $p = 0.860$), or SUVmean vs volume ($r = -0.383$, $p = 0.003$).

3.2.2. Blood

To determine if a relation exists between the findings in anatomically unaffected lung tissue and the systemic alterations detected in blood, whole blood samples were analyzed using FACS analysis. In view of the

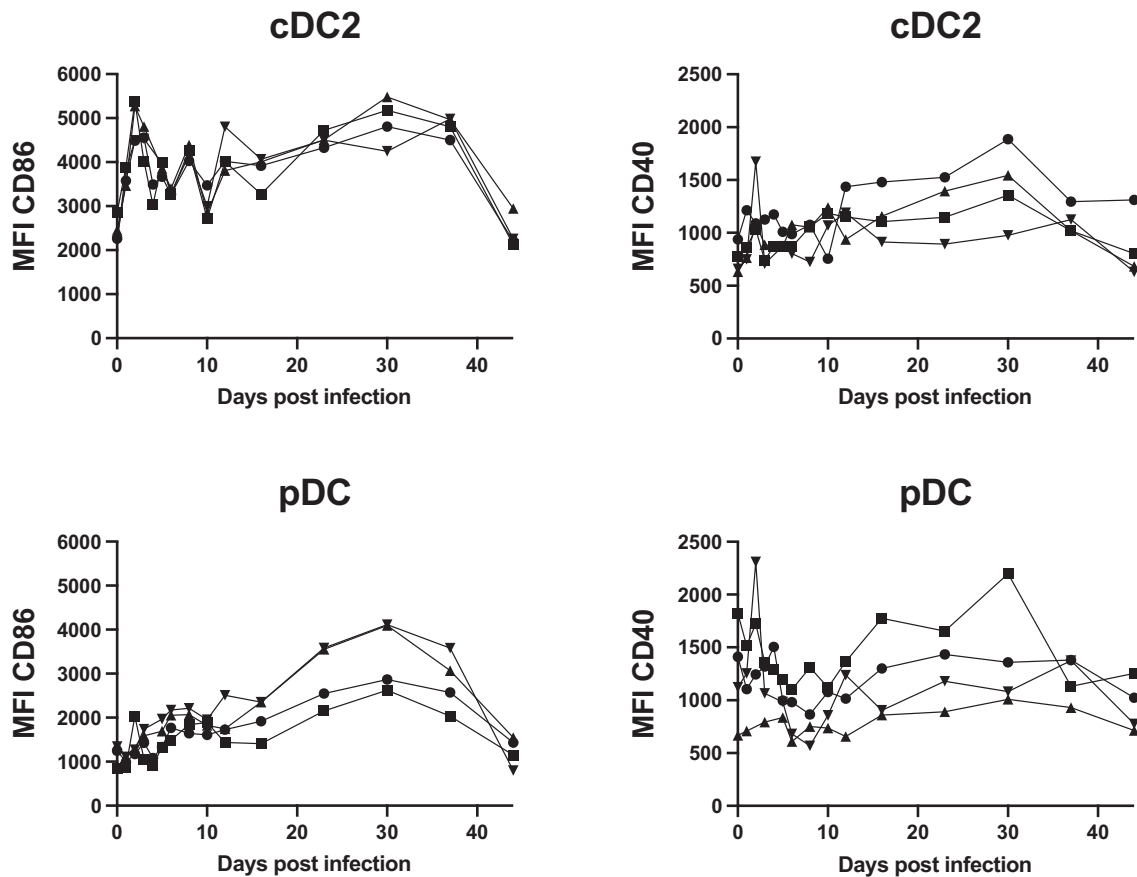


Fig. 3. FACS analysis of activation marker expression on DC in blood. Shown is the mean fluorescence intensity (MFI) of CD86 (left graphs) and CD40 (right graphs) expression on cDC2 (classical dendritic cells, top graphs) and pDC (plasmacytoid dendritic cells, bottom graphs) in time.

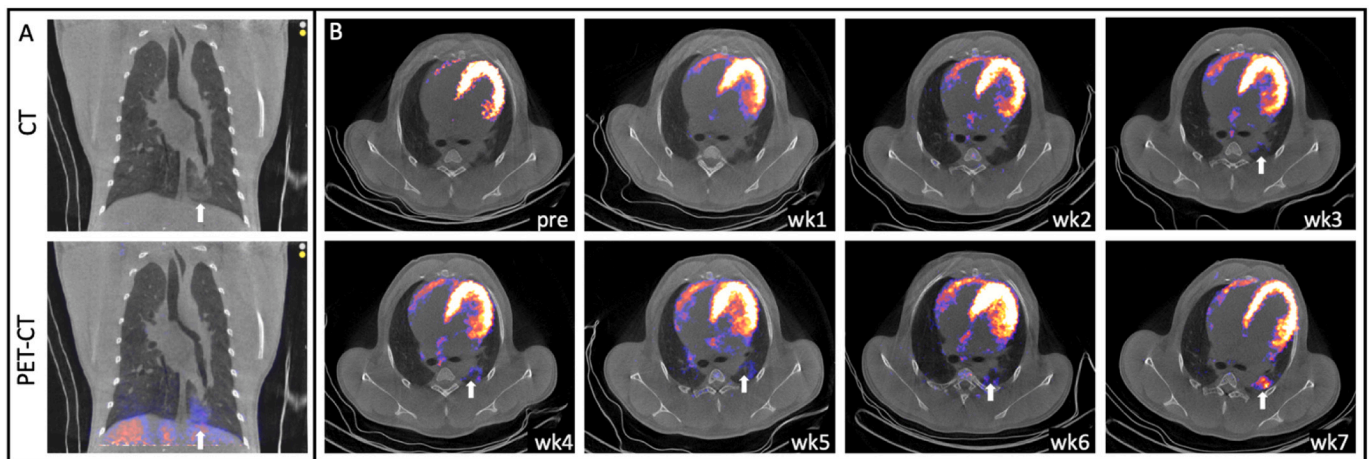


Fig. 4. Pulmonary lesion and inflammation process in a macaque after a SARS-CoV-2 infection visualized with $[^{18}\text{F}]\text{DPA714}$. A. an example of a ground glass opacity (GGO) visualized with both CT and PET-CT. B. Transversal slices of the longitudinal follow-up of one animal (inflammation process is indicated with a white arrow).

dominant expression of TSPO in monocytes, whole blood samples were analyzed for changes in monocyte and dendritic cell (DC) cell numbers, and for activation marker expression. Aside a transient increase in transitory monocytes (CD14/CD16 double positive cells), peaking at day 3–4 pi, there were no other or persistent changes measured in monocyte cell number (not shown), as also previously reported [22]. In addition, the expression of activation markers CD86 and CD40 was transiently increased, from day 2 to day 4 pi, but then returned to pre-infection levels (CD86), or showed a heterogenous pattern with increases until

day 30 pi in two out of four animals (CD40) (not shown). Instead, both the classical DC (cDC), cDC2, and the plasmacytoid DC (pDC) showed a persistently increased level of both CD86 and CD40 expression, that lasted until either day 37 pi (CD86) or day 30 pi (CD40), and then returned to the pre-infection levels (Fig. 3).

3.2.3. Pulmonary lesions and inflammation processes

All pulmonary abnormalities detected on CT coincided with an increased PET signal, also the so-called ground glass opacities which are

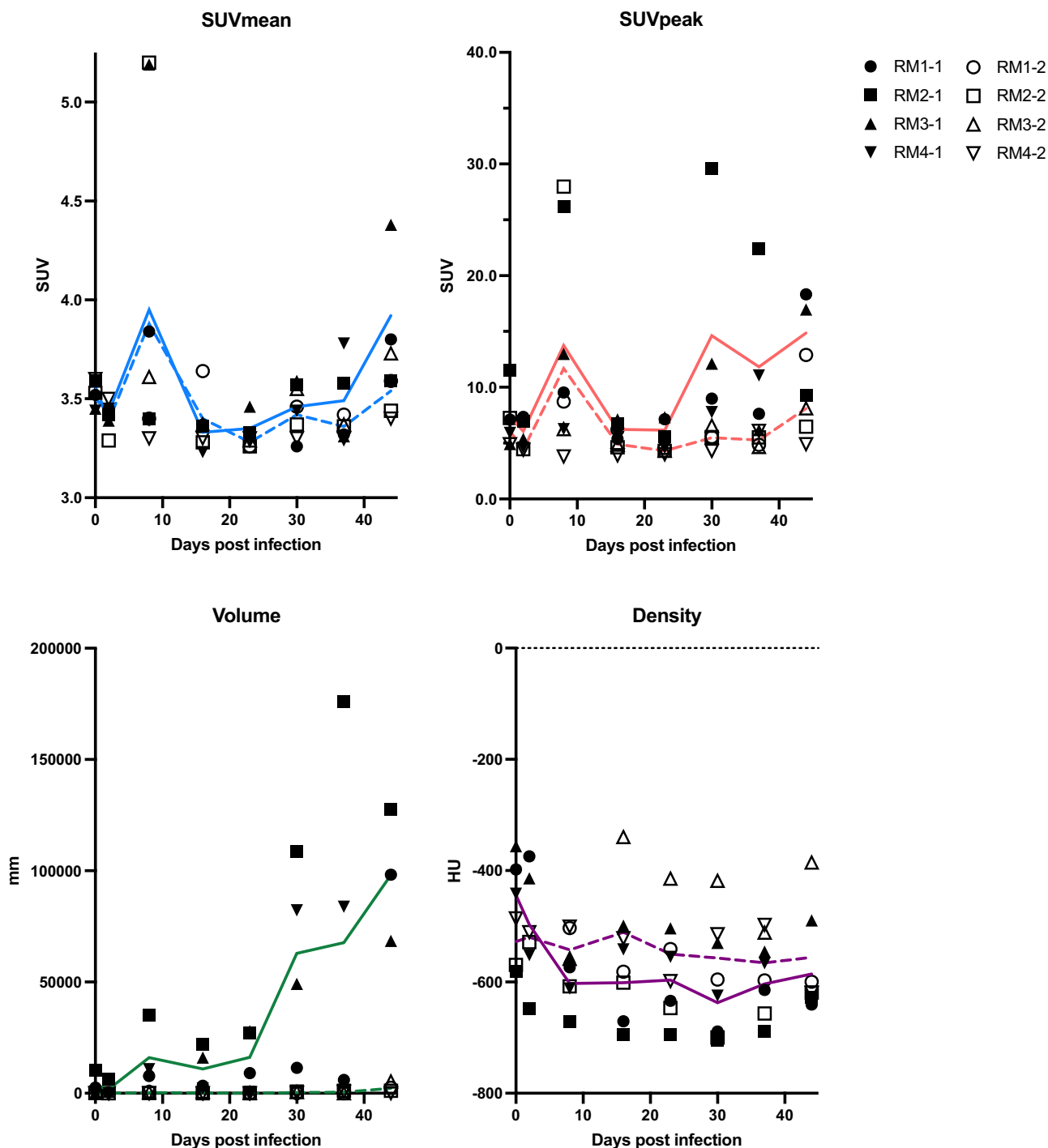


Fig. 5. Quantitative analysis of the pulmonary lesions and inflammation processes over time. The dots represent the separate animals (filled symbols = scan 1 obtained 10 min post injection, open symbols = scan 2 obtained 30 min post injection), the continuous lines represent the average of scan 1, whereas the dotted lines represent the average of scan 2.

typical lesions seen after a SARS-CoV-2 infection (Fig. 4A). In addition, the development of the lesions could be followed over time (Fig. 4B).

Besides qualitative analysis, also quantitative analyses were performed using four different variables: SUVmean, SUVpeak, density, and volume both on scan 1 and scan 2 (Fig. 5). The uptake pattern for the SUVmean was roughly the same ($p = 0.5049$) between the two scans, but only the uptake diminished over time. Also, for the SUVpeak the uptake is diminished over time, but the pattern was slightly different ($p = 0.0192$). Besides the SUVpeak, the density showed some differences too, between scan 1 and scan 2 in which the density was increased for the

second scan compared to the first scan ($p = 0.2685$). The most prominent differences between scan 1 and scan 2 were observed for the volume. The volume of the pulmonary inflammation processes was significant smaller in scan 2 versus scan 1 ($p = 0.0004$). A moderate-to-strong correlation was found between the SUVmean and SUVpeak ($r = 0.6167, p = 0.0002$), and between SUVpeak and volume ($r = 0.7841, p < 0.0001$). Only weak correlations were found between the SUVmean and volume ($r = 0.3162, p = 0.0147$), and between volume and density ($r = -0.3633, p = 0.0047$).

detection of SARS-CoV-2-induced inflammation in the pulmonary tract of rhesus monkeys. Pulmonary lesions are induced by replicating virus in the epithelial cells [15]. These activated cells may release inflammatory cytokines and chemokines that increase endothelial permeability and trigger monocyte and dendritic cell activation and recruitment into the lungs. In humans, the severity of the disease is related to levels of inflammatory cytokine production and alterations in monocyte and dendritic cell frequency and activation in both the blood and the lungs [23–25]. While expression of CD86 decreased on CDC2 and DC subsets and on monocytes in humans with severe COVID-19, we noted an upregulation of both CD86 and CD40 in the macaques. The relatively mild course of SARS-CoV-2 infection in macaques [26] might explain this different pattern of activation marker expression. The activation of these innate immune-cells could possibly contribute to the eradication of SARS-CoV-2 that was indeed shown to occur prior to onset of antigen specific T cell responses [27]. Interestingly, we observed that both increased TSPO activity as well as DC activation persisted for at least 30 days pi, despite clearance of the virus by day 10 pi. Similarly, in humans a persistent immune cell activation was reported after the clearance of SARS-CoV-2 from the body [28,29]. Persistence of antigen, autoimmunity caused by the infection, or damage repair mechanisms have been proposed as driving forces of this activation, and may also be responsible for the observation seen in the macaque model after exposure to SARS-CoV-2.

The binding affinity of [¹⁸F]DPA714, is genetically determined by a single nucleotide polymorphism rs6971 in the TSPO gene. For humans it is known that about 50% of the population is a high-affinity binder, 35% medium-affinity and 15% low-affinity [6,30]. It is unknown whether this polymorphism is human-specific or that rhesus monkeys might be affected as well. However, in cynomolgus macaques and baboons this same radioligand was tested before, resulting in high specificity binding to TSPO [5,31,32], indicating that this polymorphism is at least not present in these NHP species. This was not studied as our goal was to obtain a first proof-of-principle of visualizing the inflammation process in the entire pulmonary tract after a SARS-CoV-2 infection using [¹⁸F]DPA714. Moreover, by comparing the scan pre infection with multiple timepoints post infection, the effect of this polymorphism in rhesus monkeys is diminished. The limited number of animals used in this study is compensated by the number of scans obtained from each animal over a longer time course which makes it possible to answer the research question in this proof-of-concept study.

During this study per timepoint and per animal two single images were acquired, one in the time frame ten-twenty minutes post injection and a second in the time frame thirty-forty minutes post injection of [¹⁸F]DPA714. Both scans were analyzed, and different results were retrieved. With respect to the aim of this manuscript, which was to investigate the potential of [¹⁸F]DPA714 to visualize the inflammation process in the lungs, after exposure to SARS-CoV-2, as a proof of concept study, still important conclusions could be drawn. To determine an increased uptake of a tracer in a certain ROI there are two main parameters, besides the uptake in the target, which will assist in guiding this. The first is the target-to-background ratio and the second the uptake in the surrounding tissues. While comparing the first and second scan, the target-to-background ratio is roughly similar. However, the uptake in the surrounding tissues, the background, is lower in the second scan. For this reason, for future studies, applying an incubation time of 30 min before starting the scan is recommended. In addition, within this timeframe it is less likely that the distribution kinetics of the tracer will influence the uptake in the ROI which could lead to differences in uptake between animals.

In conclusion, despite the presence of an elevated signal in anatomically unaffected lung tissue surrounding the lung lesions, significant differences between the scans obtained before and after infection allowed us to detect not only SARS-CoV-2-associated pulmonary lesions but also inflammatory processes. In other words, abnormalities in the pulmonary tract could be detected by both CT and PET. In

addition, the inflammatory process detected in anatomically unaffected lung tissue coincided with DC activation that was detected in whole blood samples.

Our data thus indicate that [¹⁸F]DPA714 can be applied to visualize the pulmonary tract following a SARS-CoV-2 infection in rhesus monkeys. It is tempting to speculate that this methodology is applicable to other viruses causing pulmonary infections, and that this approach may be translated to the clinic as early diagnostic tracer for these indications too.

Credit authorship contribution statement

Conceptualization, LM, UF, MPJM, EJV, ADW, MAS; methodology, LM, KPB, JB, GK, PM, BEV, UF, MPJM, ADW, MAS; formal analysis, LM, GK, PM, MAS; investigation, LM, KPB, JB, DV, ZF, BEV, MAS; writing - original draft preparation, LM, GK, JAML, MAS; writing - review and editing, JB, GK, PM, JAML, EJV, MAS; supervision; JAML, EJV, ADW, MAS.

All authors have read and agreed to the published version of the manuscript.

Declaration of competing interest

The authors have no relevant financial or non-financial interests to disclose. Part of this work was supported by internal funding from the Biomedical Primate Research Centre. ADW is editor-in-chief of Nuclear Medicine and Biology and was not involved in the review of this manuscript. This publication was supported by the European Virus Archive GLOBAL (EVA-GLOBAL) project that has received funding from the European Union's Horizon 2020 research and innovation program under grant agreement No 87L029. KPB was supported by the European Union's Marie Skłodowska-Curie Innovative Training Network HONOURS; grant agreement no. 721367.

Acknowledgements

We would like to thank the Animal Science Department, especially the animal caretakers for excellent care of the animals and the Virology Department for performing the SARS-CoV-2 infection studies. We also thank Niels Beenhakker for his assistance with all the procedures regarding radioactivity, prof. Ronald Bontrop for critically reviewing the manuscript and, Francisca van Hassel for her assistance with figure editing.

References

- [1] Boszormenyi KP, Stammes MA, Fagrouch ZC, Kiemenyi-Kayere G, Niphuis H, Mortier D, et al. The post-acute phase of SARS-CoV-2 infection in two macaque species is associated with signs of ongoing virus replication and pathology in pulmonary and extrapulmonary tissues. *Viruses* 2021;13.
- [2] Arlicot N, Vercouillie J, Ribeiro MJ, Tauber C, Venel Y, Baulieu JL, et al. Initial evaluation in healthy humans of [¹⁸F]DPA-714, a potential PET biomarker for neuroinflammation. *Nucl Med Biol* 2012;39:570–8.
- [3] Chen Z, Haider A, Chen J, Xiao Z, Gobbi L, Honer M, et al. The repertoire of small-molecule PET probes for neuroinflammation imaging: challenges and opportunities beyond TSPO. *J Med Chem* 2021;64:17656–89.
- [4] Gouilly D, Saint-Aubert L, Ribeiro MJ, Salabert AS, Tauber C, Peran P, et al. Neuroinflammation PET imaging of the translocator protein (TSPO) in Alzheimer's disease: an update. *Eur J Neurosci* 2022.
- [5] Lavis S, Inoue K, Jan C, Peyronneau MA, Petit F, Goutal S, et al. [¹⁸F]DPA-714 PET imaging of translocator protein TSPO (18 kDa) in the normal and excitotoxically-lesioned nonhuman primate brain. *Eur J Nucl Med Mol Imaging* 2015;42:478–94.
- [6] Hagens MHJ, Golla SV, Wijburg MT, Yaqub M, Heijtel D, Steenwijk MD, et al. In vivo assessment of neuroinflammation in progressive multiple sclerosis: a proof of concept study with [¹⁸F]DPA714 PET. *J Neuroinflammation* 2018;15:314.
- [7] Iking J, Staniszewska M, Kessler L, Klose JM, Luckeath K, Fendler WP, et al. Imaging inflammation with positron emission tomography. *Biomedicines* 2021;9.
- [8] Goggi JL, Claser C, Hartimath SV, Hor PX, Tan PW, Ramasamy B, et al. PET imaging of translocator protein as a marker of malaria-associated lung inflammation. *Infect Immun* 2021;89:e0002421.

- [9] Foss CA, Harper JS, Wang H, Pomper MG, Jain SK. Noninvasive molecular imaging of tuberculosis-associated inflammation with radioiodinated DPA-713. *J Infect Dis* 2013;208:2067–74.
- [10] Ruiz-Bedoya CA, Mota F, Ordonez AA, Foss CA, Singh AK, Praharaj M, et al. (124I)-iodo-DPA-713 positron emission tomography in a hamster model of SARS-CoV-2 infection. *Mol Imaging Biol* 2022;24:135–43.
- [11] Imai M, Iwatsuki-Horimoto K, Hatta M, Loeber S, Halfmann PJ, Nakajima N, et al. Syrian hamsters as a small animal model for SARS-CoV-2 infection and countermeasure development. *Proc Natl Acad Sci U S A* 2020;117:16587–95.
- [12] Stammes MA, Lee JH, Meijer L, Naninck T, Doyle-Meyers LA, White AG, et al. Medical imaging of pulmonary disease in SARS-CoV-2-exposed non-human primates. *Trends Mol Med* 2022;28:123–42.
- [13] Casel MAB, Rollon RG, Choi YK. Experimental animal models of coronavirus infections: strengths and limitations. *Immune Netw* 2021;21:e12.
- [14] Cleary SJ, Pitchford SC, Amison RT, Carrington R, Robaina Cabrera CL, Magnen M, et al. Animal models of mechanisms of SARS-CoV-2 infection and COVID-19 pathology. *Br J Pharmacol* 2020;177:4851–65.
- [15] Kosyreva A, Dzhaliylova D, Lokhonina A, Vishnyakova P, Fatkhudinov T. The role of macrophages in the pathogenesis of SARS-CoV-2-associated acute respiratory distress syndrome. *Front Immunol* 2021;12:682871.
- [16] Maaskant A, Meijer L, Fagrouch Z, Bakker J, van Geest L, Zijlmans DGM, et al. Bronchoalveolar lavage affects thorax computed tomography of healthy and SARS-CoV-2 infected rhesus macaques (*Macaca mulatta*). *PLoS One* 2021;16:e0252941.
- [17] Singletary ML, Phillippi-Falkenstein KM, Scanlon E, Bohm Jr RP, Veazey RS, Gill AF. Modification of a common BAL technique to enhance sample diagnostic value. *J Am Assoc Lab Anim Sci* 2008;47:47–51.
- [18] Mooij P, Koopman G, Mortier D, van Heteren M, Oostermeijer H, Fagrouch Z, et al. Pandemic swine-origin H1N1 influenza virus replicates to higher levels and induces more fever and acute inflammatory cytokines in cynomolgus versus rhesus monkeys and can replicate in common marmosets. *PLoS One* 2015;10:e0126132.
- [19] Golla SS, Boellaard R, Oikonen V, Hoffmann A, van Berckel BN, Windhorst AD, et al. Quantification of [18F]DPA-714 binding in the human brain: initial studies in healthy controls and Alzheimer's disease patients. *J Cereb Blood Flow Metab* 2015;35:766–72.
- [20] Stammes MA, Bakker J, Vervenne RAW, Zijlmans DGM, van Geest L, Vierboom MPM. In: Recommendations for Standardizing Thorax PET-CT in Non-Human Primates by Recent Experience from Macaque Studies Animals; 2021. p. 11.
- [21] Tölgyesi B, Bakker J, Nagy K, Meijer L, van Geest L, Stammes MA. Refined acquisition of high-resolution thorax CTs in macaques by free breathing Laboratory Animals. 2021.
- [22] Mooij P, Garcia-Arriaza J, Pérez P, Lázaro-Frias A, Verstrepen BE, Böszörményi KP. Poxvirus MVA expressing SARS-CoV-2 S protein induces robust immunity and protects rhesus macaques from SARS-CoV-2. *Front Immunol* 2022:13.
- [23] Kvedaraitė E, Hertwig L, Sinha I, Ponzetta A, Hed Myrberg I, Lourda M, et al. Major alterations in the mononuclear phagocyte landscape associated with COVID-19 severity. *Proc Natl Acad Sci U S A* 2021;118.
- [24] Liao M, Liu Y, Yuan J, Wen Y, Xu G, Zhao J, et al. Single-cell landscape of bronchoalveolar immune cells in patients with COVID-19. *Nat Med* 2020;26:842–4.
- [25] Winheim E, Rinke L, Lutz K, Reischer A, Leutbecher A, Wolfram L, et al. Impaired function and delayed regeneration of dendritic cells in COVID-19. *PLoS Pathog* 2021;17:e1009742.
- [26] Munoz-Fontela C, Dowling WE, Funnell SGP, Gsell PS, Riveros-Balta AX, Albrecht RA, et al. Animal models for COVID-19. *Nature* 2020;586:509–15.
- [27] Nelson CE, Namasivayam S, Foreman TW, Kauffman KD, Sakai S, Dorosky DE, et al. Mild SARS-CoV-2 infection in rhesus macaques is associated with viral control prior to antigen-specific T cell responses in tissues. *Sci Immunol* 2022:eabo0535.
- [28] Phetsouphanh C, Darley DR, Wilson DB, Howe A, Munier CML, Patel SK, et al. Immunological dysfunction persists for 8 months following initial mild-to-moderate SARS-CoV-2 infection. *Nat Immunol* 2022;23:210–6.
- [29] Ryan FJ, Hope CM, Masavuli MG, Lynn MA, Mekonnen ZA, Yeow AEL, et al. Long-term perturbation of the peripheral immune system months after SARS-CoV-2 infection. *BMC Med* 2022;20:26.
- [30] Owen DR, Gunn RN, Rabiner EA, Bennacef I, Fujita M, Kreisler WC, et al. Mixed-affinity binding in humans with 18-kDa translocator protein ligands. *J Nucl Med* 2011;52:24–32.
- [31] Saba W, Goutal S, Auvity S, Kuhnast B, Coulon C, Kouyoumdjian V, et al. Imaging the neuroimmune response to alcohol exposure in adolescent baboons: a TSPO PET study using (18) F-DPA-714. *Addict Biol* 2018;23:1000–9.
- [32] Saba W, Goutal S, Kuhnast B, Dolle F, Auvity S, Fontyn Y, et al. Differential influence of propofol and isoflurane anesthesia in a non-human primate on the brain kinetics and binding of [(18)F]DPA-714, a positron emission tomography imaging marker of glial activation. *Eur J Neurosci* 2015;42:1738–45.